PCCP

ROYAL SOCIETY OF CHEMISTRY

PAPER

View Article Online
View Journal

Cite this: DOI: 10.1039/d6cp00658b

Combining photo-CIDNP and long-lived spin states enables high-contrast detection of weak protein–ligand interactions

Matthias Bütikofer, [ac] Anna Sonnefeld, [b] Gabriela R. Stadler, [a] Felix Torres, [c] Geoffrey Bodenhausen, [b] Kirill F. Sheberstov *[b] and Roland Riek *[a]

Received 23rd February 2026,
Accepted 1st May 2026

DOI: 10.1039/d6cp00658b

rsc.li/pccp

Photo chemically induced dynamic nuclear polarization (photo-CIDNP) and long-lived spin states (LLS) are two nuclear magnetic resonance (NMR) techniques that can be combined to achieve large signal enhancements and extended lifetimes of spin order, respectively, and their combination is useful for detecting biomolecular interactions. Here, we demonstrate that integrating photo-CIDNP hyperpolarization with LLS excitation through spin-lock induced crossing (SLIC) enables the highly sensitive detection of signals of ligands at micromolar concentrations. Using indole-3-propionic acid (IPA), we show that two of its CH_2 protons are simultaneously suitable for efficient photo-CIDNP polarization and for SLIC-based singlet excitation, thus allowing the conversion of hyperpolarized Zeeman order into long-lived singlet order. The resulting CIDNP-LLS approach provides a signal-to-noise enhancement of up to 30-fold over conventional LLS, enabling the detection of 25 μM IPA in a 3 mm tube within two scans. In the presence of the enzyme arylalkylamine *N*-acetyltransferase (AANAT) at a 100 nM concentration, CIDNP-LLS offers superior binding contrast compared to conventional CIDNP or CIDNP combined with perfect echo refocusing (CIDNP-PEARLScreen), making it a powerful method for monitoring weak protein–ligand interactions.

Introduction

Nuclear magnetic resonance (NMR) spectroscopy is one of the most powerful and versatile analytical techniques in chemistry and structural biology, providing atomic-resolution information on molecular structure, dynamics, and interactions. However, NMR suffers from inherently low sensitivity, arising from the small energy difference between nuclear spin states, which results in only a tiny population difference at thermal equilibrium, typically on the order of parts per million at standard magnetic field strengths. This sensitivity limitation restricts the applicability of NMR, particularly for samples available only at low concentrations, such as biomolecular targets relevant to drug discovery. Hyperpolarization methods have emerged as a powerful strategy to overcome this barrier, generating non-equilibrium nuclear spin polarization that can exceed thermal levels by several orders of magnitude. Among the most widely used approaches are dynamic nuclear polarization (DNP),[1] para-hydrogen-induced polarization (PHIP),[2] signal amplification by reversible exchange (SABRE),[3] and photochemically induced dynamic nuclear polarization (photo-CIDNP),[4,5] each offering distinct advantages in terms of applications to various molecules, hardware requirements, costs, and experimental accessibility.[6]

However, hyperpolarized spin order is still subject to longitudinal relaxation, decaying with T_1, which can be on the order of seconds for small molecules. Long-lived spin states (LLS) offer a solution to this limitation, providing spin states with lifetimes T_{LLS} that can substantially exceed T_1 by exploiting the fact that some relaxation pathways are forbidden by symmetry in near-equivalent spin pairs.[7,8]

Long-lived states (LLS) have a growing impact on drug discovery and molecular screening, as the LLS lifetimes T_{LLS} decrease upon ligand interaction with the environment (*e.g.*, a protein binding pocket), enabling the observation of binding between proteins and small molecules. Indeed, it has been shown that ^1H or ^{19}F LLS can be used for detecting binding between small ligands and macromolecular targets.[9–11] Furthermore, because the contrast of LLS lifetimes

[a] *Institute of Molecular Physical Science, ETH Zürich, Vladimir-Prelog-Weg 2, CH-8093 Zürich, Switzerland. E-mail: roland.riek@phys.chem.ethz.ch*
[b] *Chimie Physique et Chimie du Vivant (CPCV, UMR 8228), Department of Chemistry, Ecole Normale Supérieure, PSL University, Sorbonne University, CNRS, Paris, 75005, France. E-mail: kirill.sheberstov@ens.psl.eu*
[c] *NexMR AG, Wiesenstrasse 10A, 8952 Schlieren, Switzerland. E-mail: ftorres@nexmr.com*

caused by binding is independent of the molecular weight of the macromolecular target and because the ligand signal can be studied for longer times than responses limited by T_1, LLS are of particular interest for low-molecular-weight targets, provided the fast exchange condition is fulfilled.

LLS are typically excited in isolated pairs of spins-1/2, where they can be defined as population imbalances between the mean populations of the triplet states T_{+1}, T_0, and T_{-1}, and the singlet state S_0.[8] The extended lifetimes of LLS are due to the fact that the intra-pair dipole–dipole mechanism, which can be a dominant contributor to T_1 relaxation, cannot relax singlet–triplet population imbalances. Long-lived states can also be excited in spin systems containing more than two spins-1/2,[12–14] for example, in aliphatic moieties containing magnetically inequivalent methylene protons.[15] Such spin systems contain pairs of strongly coupled spins, making spin-lock induced crossing (SLIC)[16] well-suited for the excitation of LLS.[17]

A challenge for SLIC-LLS applied to aliphatic chains is its relatively low sensitivity, due to the limited yield of the conversion of magnetization into LLS. The combination of hyperpolarization with LLS is therefore an attractive approach, as it simultaneously addresses the sensitivity and timescale limitations of conventional NMR. Indeed, it has been demonstrated how LLS can be used to store hyperpolarization achieved by dissolution dynamic nuclear polarization (dissolution-DNP).[18,19] Additionally, Razanahoera and coworkers have recently shown how bullet-DNP can be used to boost LLS signals observed by SLIC when deviating from the high spin temperature approximation, and propose this combination of methods to detect protein-ligand binding.[20] Since DNP platforms are engineering-heavy and complex to operate, they are not easily accessible for high-throughput or routine NMR applications.

In contrast, photo-CIDNP provides an inexpensive, easy-to-implement, widely available method for hyperpolarization. This technique relies on light pulses with a length of typically a few seconds in continuous-wave mode (CW photo-CIDNP), using suitable dyes to create transient radical-pair reactions that can induce strong nuclear polarization.[4,5,21] The chemical space accessible to photo-CIDNP has been substantially expanded in recent years, thereby enabling rapid and robust screening for fragment-based drug discovery (FBDD) workflows.[22–25] Photo-CINDP can enhance signals by up to 3 orders of magnitude using standard NMR hardware.[26] Photo-CIDNP has previously been shown to generate heteronuclear singlet order in ^{1}H–^{13}C spin pairs under zero- to ultralow-field conditions, demonstrating that photo-CIDNP and singlet order can in principle be combined.[27]

Building on these advances, this work introduces the first combination of photo-CIDNP and SLIC-LLS (CIDNP-LLS). We demonstrate a proof of concept for this approach, selectively detecting long-lived states of the $CH_2^{(4)}$ group of indole-3-propionic acid (IPA), and applying CIDNP-LLS to reveal the binding interaction of the ligand IPA with the target arylalkylamine *N*-acetyltransferase (AANAT),[28] with a dissociation constant K_D in the low millimolar regime. The performance of CIDNP-LLS is compared to established methods, including conventional CIDNP binding assays and the recently introduced PEARLScreen method,[29] which can also be boosted by CIDNP, as shown in this work. This highlights the advantages of CIDNP-LLS for increased binding sensitivity in the context of drug discovery and FBDD.

Results and discussion

Photo-CIDNP enhancement of IPA magnetization and its conversion into LLS

Aromatic amino acids and their analogues, such as tryptophan, tyrosine, and indole derivatives, are well known for their strong photo-CIDNP hyperpolarization.[22,30] Among these, indole-3-propionic acid (IPA) serves as a particularly suitable model compound because the indole $CH_2^{(4)}$ protons exhibit a large CIDNP enhancement and form a chemically equivalent, but magnetically inequivalent spin pair, because of the adjacent $CH_2^{(5)}$ protons, making them suitable for SLIC.[17]

Upon 520 nm CW laser irradiation in the presence of 20 μM fluorescein, the CIDNP-1D ^{1}H NMR (CIDNP-1D) signal of $CH_2^{(4)}$ of IPA was enhanced approximately 30-fold compared to its thermal intensity (Fig. 1A). A strong hyperpolarization of $CH_2^{(4)}$ was expected, as this methylene position is directly adjacent to the aromatic ring and therefore experiences large hyperfine couplings, consistent with the well-established CIDNP behavior of tryptophan and its analogues. In contrast, $CH_2^{(5)}$, being one carbon further removed from the ring, exhibits significantly weaker hyperfine couplings and consequently only a modest CIDNP enhancement.[31]

For the SLIC pulse, the optimal amplitude is ν_{SLIC} = 29.5 Hz while the optimal pulse duration is 250 ms. Under these conditions, an LLS-derived thermal signal was observed for $CH_2^{(4)}$, as shown in the grey spectrum of Fig. 1B.

When the SLIC experiment was preceded by laser irradiation to combine photo-CIDNP hyperpolarization with LLS excitation (CIDNP-SLIC), a substantial gain in sensitivity was obtained. The resulting spectrum in Fig. 1B (black trace) exhibits a signal-to-noise enhancement of approximately 32-fold compared to the SLIC-derived spectrum without CIDNP (grey). Using only 25 μM IPA in a 3 mm NMR tube with merely two scans, CIDNP-LLS signals with a signal-to-noise ratio S/N = 19 could be detected for an LLS-relaxation time τ_{LLS} = 0.1 s, decreasing to S/N = 7 after τ_{LLS} = 5 s (Fig. 1C). This clearly demonstrates that CIDNP hyperpolarization can overcome the intrinsic sensitivity limitations of SLIC-based methods. These results establish IPA as a suitable system for a proof-of-concept, as it simultaneously fulfills the two key requirements of being both ''CIDNPable'' and ''SLICable.'' In the future, this limitation could be mitigated either by expanding the scope of photo-CIDNP through the development of new dye-molecule combinations or by coupling photo-CIDNP to alternative LLS excitation schemes, which allow the excitation of LLS in spin pairs that are not chemically equivalent. However, such approaches often require continuous RF irradiation or other spin-locking schemes to

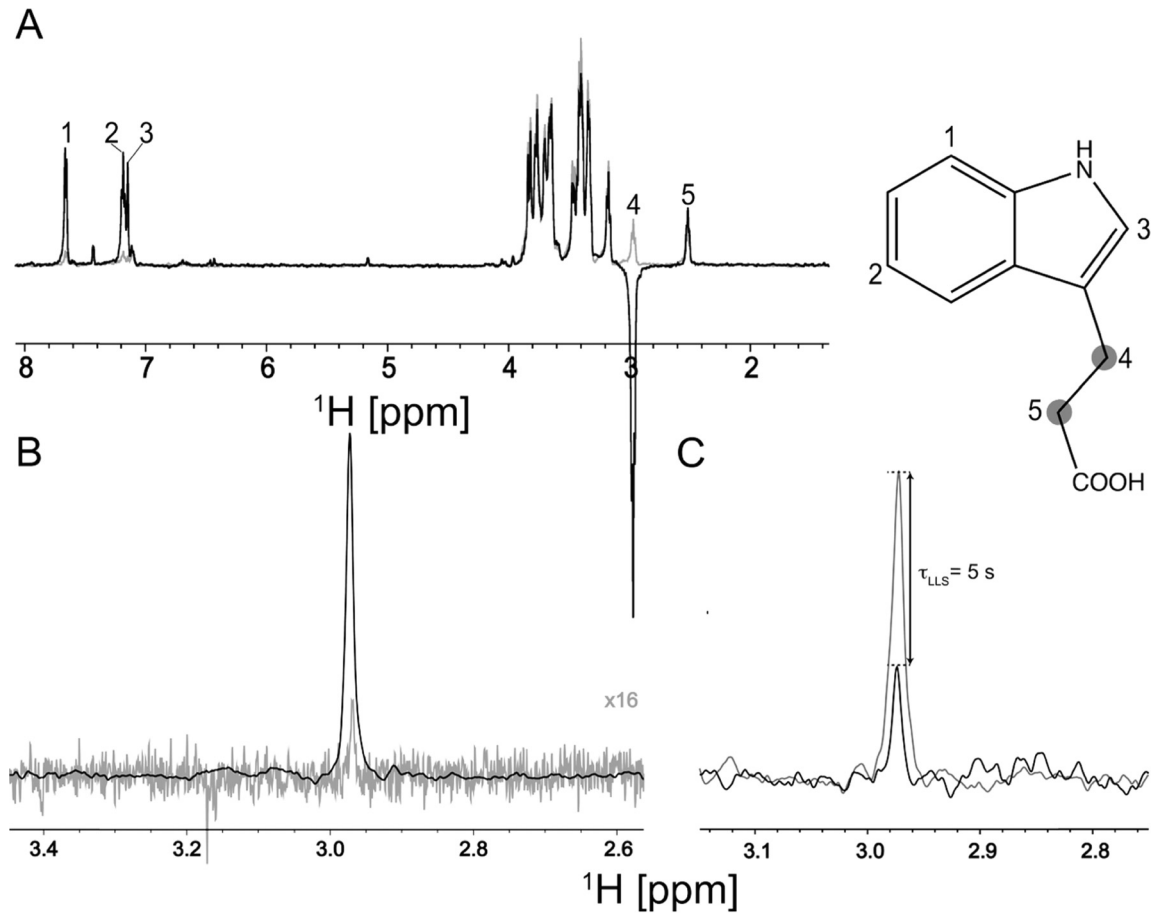

Fig. 1 Amplified detection of LLS of indole-3-propionic acid (IPA) using photo-CIDNP. (A) CIDNP-1D spectrum of 500 μM IPA recorded without (grey) and with laser irradiation of 2 s (black). The $CH_2^{(4)}$ group that exhibits a strong CIDNP enhancement (grey dots on the molecular structure of IPA) is also accessible for LLS excitation by SLIC. (B) Comparison of LLS spectra of the $CH_2^{(4)}$ group of 500 μM IPA recorded starting with thermal Boltzmann polarization (scaled 16x, grey, 4 scans), and boosted by photo-CIDNP (not scaled, black, 2 scans). Both spectra were recorded with a relaxation delay τ_{LLS} = 0.1 s. (C) CIDNP-LLS signal of $CH_2^{(4)}$ using 25 μM IPA (3 mm tube, 2 scans) for τ_{LLS} = 0.1 s (grey) and τ_{LLS} = 5 s (black). No signal could be observed using the same setup without CIDNP.

sustain the singlet order. Spin pairs close to equivalence do not require any sustaining. In addition, SLIC allows LLS excitation of several molecules in mixtures simultaneously.[17] After showing the proof-of-concept that one can obtain a hyperpolarized LLS-derived signal using photo-CIDNP, we verified that the LLS lifetime is the same for thermal and CIDNP polarization.

LLS lifetime of IPA under thermal and CIDNP conditions

Using a 5 mM IPA sample, the decay of the LLS excited in IPA was compared with a conventional T_1 inversion-recovery experiment. As shown in Fig. 2A, the LLS decay (T_{LLS} = 10.1 s) is significantly longer than T_1 = 1.3 s, confirming the formation of a state with an extended lifetime, with a ratio T_{LLS}/T_1 = 7.8.

To investigate the relaxation properties of LLS in IPA, relaxation experiments were performed under both thermal and photo-CIDNP conditions (Fig. 2). The presence of the dye might have a deleterious effect on the lifetime, for example, if IPA could form a complex with the fluorescein dye. When repeating the same measurement under photo-CIDNP conditions (CIDNP-LLS) at a 100-fold lower concentration ([IPA] = 50 μM), a similar mono-exponential relaxation behavior was observed (Fig. 2B). A conventional inversion-recovery experiment performed with thermal polarization on the same 50 μM sample yielded T_1 = 1.4 s (Fig. S2), consistent with the value measured at 5 mM. However, a signal-to-noise ratio of only 13 was achieved with 8 scans, highlighting that significantly more scans would be required to obtain data of comparable quality to that of the CIDNP approach. The comparison of thermal-LLS and CIDNP-LLS decays underscores that the underlying singlet relaxation properties of IPA are essentially preserved under hyperpolarizing conditions. However, the progressive bleaching of the photosensitizer upon repeated laser irradiation turns out to be the main factor limiting the accuracy and dynamic range of conventional CIDNP-LLS relaxation experiments. Bleaching leads to an accelerated apparent signal decay that is unrelated to intrinsic LLS relaxation and must be considered for quantitative analysis. Strategies to alleviate bleaching, such as interleaved acquisition schemes (as used in this work) or the use of sacrificial reductants and radical quenchers (*e.g.*, ascorbate, also known as vitamin C), are therefore relevant for real-world implementations since such reagents may extend the

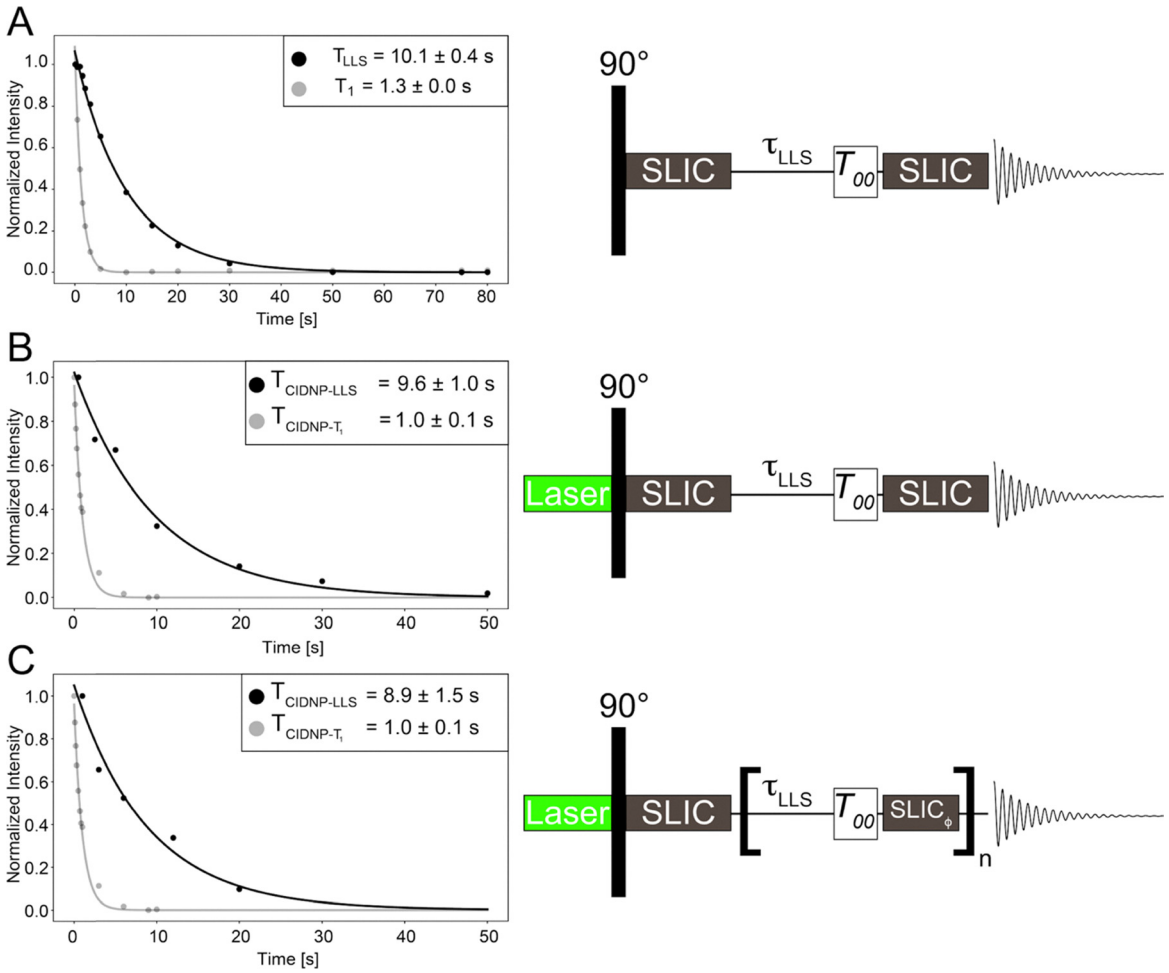

Fig. 2 CIDNP-SLIC pulse sequences. (A) LLS relaxation decay using thermal polarization SLIC-LLS pulse sequence (5 mM IPA, 5 mm NMR tube) compared with a T_1 inversion-recovery experiment. The T_1 inversion-recovery curve was normalized and inverted to match the decay of the LLS curve, allowing direct visual comparison of the two timescales. (B) CIDNP-LLS relaxation of 50 μM IPA (3 mm tube) obtained by pulse sequence shown on the right-hand side. The pulse sequence used to measure the CIDNP-T_1 is shown in SI Fig. S1. (C) CIDNP-LLS decay detected "on-the-fly" for 50 μM IPA (3 mm tube) using a CIDNP-LLS pulse sequence, where the SLIC pulse used to convert LLS into observable magnetization is shortened by a factor N = 5 to reconvert only a fraction of the LLS.

time window of CIDNP-LLS experiments.[32] Here, we propose a different method, using "on-the-fly" CIDNP-LLS measurements. As has been demonstrated for bullet-DNP,[20] the reconversion SLIC pulse can be shortened from the optimum τ_{SLIC}^{opt} to τ_{SLIC}^{opt}/N so that only a fraction of the LLS is converted into observable magnetization. This allowed "on-the-fly" monitoring of the relaxation of the LLS within a single scan (Fig. 2C). However, the method suffers from losses of signal-to-noise compared to the conventional step-by-step approach.

Comparing CIDNP-PEARLScreen and CIDNP-LLS for the detection of protein–ligand binding

The enhanced sensitivity of CIDNP-LLS was exploited to probe the interaction between the ligand IPA and the protein target dopamine arylalkylamine *N*-acetyltransferase (AANAT), a small enzyme (25 kDa) involved in melatonin biosynthesis.[28] We showed in previous studies how CIDNP-1D can be used to detect binding (pulse sequence in SI Fig. S1A).[23] The PEARLScreen experiment has recently been introduced as a sensitive method for ^{1}H-screening.[29] In this work, we show for the first time how CIDNP can be combined with PEARLScreen to detect the CIDNP signal attenuation through selective relaxation and the enhanced T_2 relaxation upon binding in a sequence of experiments (SI Fig. S1B). Fig. 3 compares the effect of AANAT addition on the IPA signals by measuring either CIDNP-PEARLScreen or CIDNP-LLS.

In the fast-exchange regime, binding-induced NMR contrast is governed by the population-weighted averaging of relaxation rates, as described by Salvi *et al.*,[9] where contrast is defined in terms of changes in relaxation rates $\langle R_i \rangle$ between free and bound ligand states. As the rate-based formulation requires access to full relaxation decay curves, which is often impractical in drug discovery applications, we introduce the single-point intensity-based binding contrast parameter C_{Bind}, defined as:

$$C_{Bind} = \frac{I_{t,+P}}{I_{t,free}} \quad (1)$$

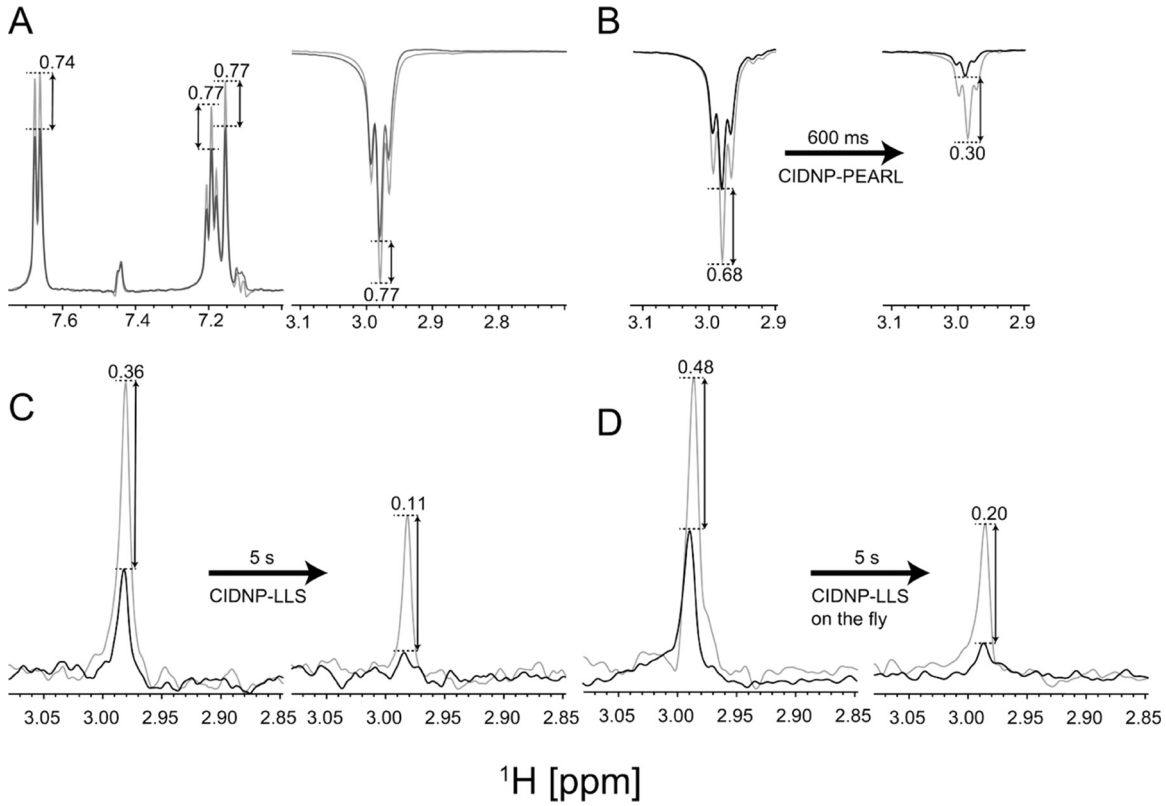

Fig. 3 Signal reduction of $CH_2^{(4)}$ signals of IPA upon addition of the protein AANAT using CIDNP-1D, CIDNP-PEARLScreen, and CIDNP-LLS. Each spectrum represents 200 μM IPA in the absence (grey) and the presence (black) of 10 μM AANAT. Arrows indicate the intensity drop upon protein addition, and the numbers show the intensity ratios of the signal in the presence and absence of the protein (C_{Bind}). (A) Single scan CIDNP-1D spectra of the aromatic and aliphatic regions using 2 s laser irradiation. (B) CIDNP-PEARLScreen spectra (only $CH_2^{(4)}$ shown) with relaxation delays τ_{CPMG} = 0 and 600 ms using the pulse sequence shown in Fig. S1B of the SI. The sample was irradiated for 2 s with a CW laser (1.6 W, 520 nm) before each scan. (C) CIDNP-LLS spectra with τ_{LLS} = 0.25 and 5 s, using the pulse sequence shown in Fig. 1B. The sample was irradiated for 1 s with a laser irradiation before each scan, and 2 scans were averaged. (D) "On-the-fly" CIDNP-LLS with τ_{LLS} = 0.25 and 5 s, using the pulse sequence shown in Fig. 1B. 16 scans were acquired, and the sample was irradiated with the laser for 2 s before each scan.

where $I_{t,+P}$ and $I_{t,free}$ denote the ligand signal intensities at a given relaxation delay t in the presence and absence of protein, respectively. For experiments that provide two relaxation delays (*e.g.* PEARLScreen and SLIC), we follow the established notation of the ligand score Q:[29]

$$Q = \frac{I_{t\,max,+P} I_{t\,min,free}}{I_{t\,min,+P} I_{t\,max,free}} \quad (2)$$

where the ratio is calculated between two normalized intensities at time points t_{min} and t_{max} (*e.g.*, for minimal and maximal relaxation delays).

In all cases, a decrease in the IPA signal intensity was observed when [AANAT] = 10 μM was added to [IPA] = 200 μM, indicating binding between ligand and protein. The binding was confirmed with [^{15}N, ^{1}H]-HSQC chemical shift perturbation experiments (see Fig. S3 in SI), which allowed us to define an affinity with K_D = 1.7 mM.

As shown in Fig. 3A, CIDNP-1D spectra exhibited only moderate changes (C_{Bind} = 0.77 for $CH_2^{(4)}$), whereas CIDNP-PEARLScreen (Fig. 3B) and CIDNP-LLS (Fig. 3C and D) provided significantly higher contrast. For the $CH_2^{(4)}$ resonance of IPA, C_{Bind} decreased to 0.3 for τ_{CPMG} = 600 ms, resulting in Q = 0.44 using CIDNP-PEARLScreen.

In contrast, CIDNP-LLS, measured both step-by-step and on-the-fly, revealed a strong contrast even at short LLS delays (τ_{LLS} = 0.25 s) with respective C_{Bind} values of 0.36 and 0.48. After a delay τ_{LLS} = 5 s, these dropped to 0.11 or 0.2, respectively (Q = 0.31 or Q = 0.42). The pronounced initial signal attenuation reflects not only enhanced relaxation of the long-lived state upon binding but also the fact that CIDNP-LLS uses a relatively long SLIC excitation period (τ_{SLIC} = 250 ms), during which relaxation is affected by the protein.

These results demonstrate that boosting LLS by CIDNP can effectively bridge the sensitivity issues that have so far limited the use of LLS for drug screening applications. The pronounced contrast Q observed for CIDNP-LLS is probably not primarily governed by T_2 or NOE-based relaxation pathways, but rather by changes in local symmetry, dynamics, and exchange processes.[33] The distinct mechanisms may explain the better performance of CIDNP-LLS and highlights its potential utility in cases where conventional relaxation-based methods become less discriminative.

CIDNP-LLS shows the highest binding contrast at low protein concentrations

To illustrate the sensitivity of CIDNP-LLS to ligand-protein binding, the LLS decays obtained for [IPA] = [L] = 200 μM and various AANAT concentrations were fitted to mono-exponential functions (titration of Fig. 4A). Even for a very low concentration [AANAT] = 100 nM, a significant relaxation enhancement is observed (T_{LLS}^{P+} = 7.83 ± 1.34 s < T_{LLS}^{free} = 11.09 ± 1.93 s). In the presence of [AANAT] = 10 μM, the lifetime decreases to T_{LLS}^{P+} = 2.95 ± 0.53 s. Note that for a relaxation period τ_{LLS} > 10 s, it is impossible to detect any LLS-derived signals.

The binding contrast can be compared for (i) CIDNP-1D enhanced conventional spectra, (ii) CIDNP-enhanced perfect echoes (CIDNP-PEARLScreen), (iii) CIDNP-LLS by using C_{Bind} or Q: C_{Bind} for the CIDNP-1D experiment was calculated according to eqn (1). Eqn (2) was used to determine Q for CIDNP-PEARLScreen and CIDNP-LLS. Either 0 or 20 refocusing cycles (SI Fig. S1B) with a spacing of t = 5 ms were used, resulting in a total relaxation delay t_{CPMG} of t_{min} = 0 ms or t_{max} = 400 ms. The longest delay was chosen to be on the order of half of the transverse relaxation time of the free ligand ($T_{2,free}$ = 1.2 s).

For the LLS experiments, storage delays of τ_{LLS} = 5 s and 10 s were used, corresponding approximately to 0.5*$T_{LLS,\ free}$ and $T_{LLS,\ free}$, respectively. As illustrated in Fig. 4, a binding contrast for all three methods is visible at [AANAT] = 10 μM. At low protein concentrations, the binding contrast for LLS is clearly superior to the other methods, regardless of relaxation delay. At low protein concentrations, the difference between τ_{LLS} = 5 s and τ_{LLS} = 10 s is relatively small within the experimental uncertainty. This is mainly due to the reduced signal-to-noise ratio at long storage delays, which leads to larger error bars and limits the precision of the extracted contrast values. In the range 0.1 < [AANAT] < 1 μM, little contrast is visible for the CIDNP-1D or CIDNP-PEARLScreen methods, but Q < 0.8 for CIDNP-LLS.

The titrations in Fig. 4 highlight the central advantage of CIDNP-LLS for binding detection: the gain in contrast at low protein concentrations, where conventional CIDNP and CIDNP-PEARLScreen show poorer contrast. A practical trade-off of this approach is that full LLS decay curves inherently require longer experimental times than T_2-based methods, simply because the LLS decays more slowly. However, as is common in fragment-based screening, the acquisition time can be significantly reduced by sampling only a minimal number of τ_{LLS} delays (*e.g.*, a single short and a single long delay τ_{LLS}) instead of recording a complete relaxation curve. In combination with CIDNP hyperpolarization, this strategy retains much of the enhanced binding contrast while keeping the overall experiment time compatible with the demands of NMR screening. Thus, although CIDNP-LLS introduces some additional complexity compared to standard CIDNP-1D or CIDNP-PEARL, its enhanced binding contrast makes it a promising addition to the toolbox of NMR-based drug discovery.

Conclusion and outlook

The present work demonstrates the feasibility of combining photo-CIDNP and LLS excitation to enhance the sensitivity of

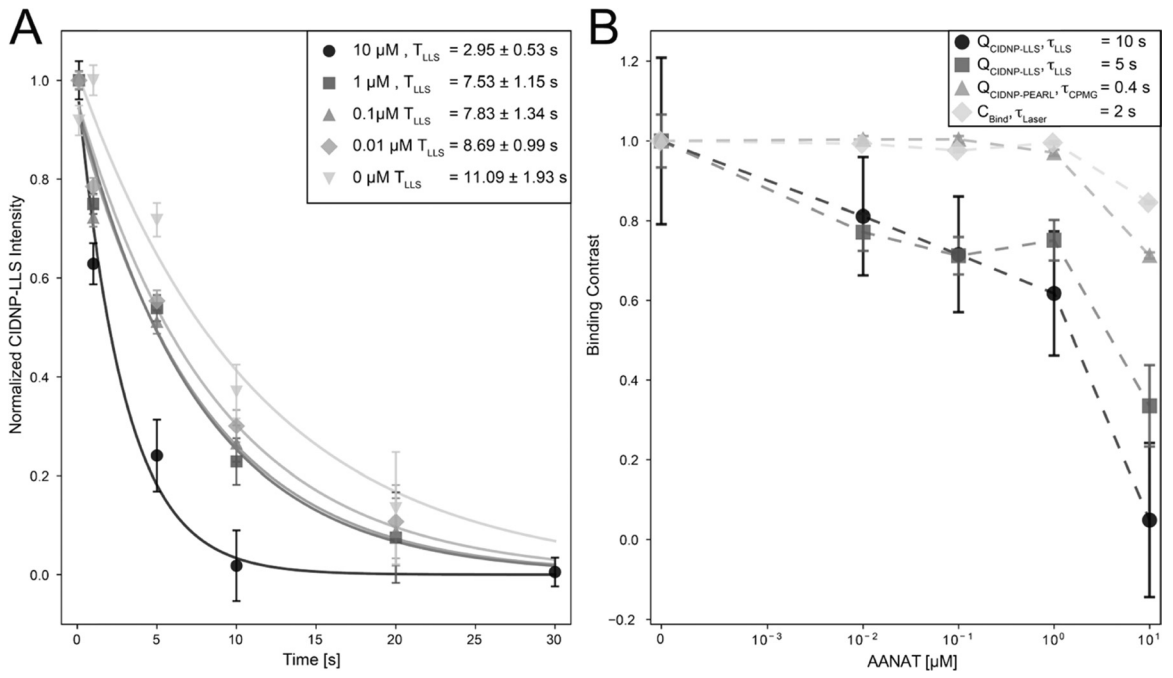

Fig. 4 Binding contrast of CIDNP-1D, CIDNP-PEARLScreen, and CIDNP-LLS as a function of the concentration of the protein AANAT. (A) Normalized CIDNP-LLS relaxation decay curves of 200 μM IPA recorded with different AANAT concentrations. Data were fitted to mono-exponentially decaying functions. Error bars represent the signal-to-noise ratio (SNR). (B) Contrast parameters C_{Bind} (eqn (1)) for CIDNP measurements and Q (eqn (2)) for CIDNP-PEARLScreen and CIDNP-LLS measurements for different AANAT concentrations.

SLIC-LLS and detect LLS at micromolar ligand and nanomolar protein concentrations. This enables the detection of weak protein–ligand interactions with higher binding contrast than established NMR methods such as CIDNP-1D or PEARLScreen.[23,29] The approach benefits from the complementary advantages of both techniques: photo-CIDNP provides rapid, non-invasive hyperpolarization only requiring an inexpensive light source and a compatible dye-molecule pair, while LLS offers slow relaxation and sensitivity to molecular symmetry and dynamics, being sensitive to minor changes in the molecular environment of the long-lived state over a time window that is longer than in conventional NMR methods.

Although CIDNP-LLS provides better binding contrast than established CIDNP-1D and PEARLScreen, these and other screening methods, such as STD-NMR[34] or WaterLOGSY,[35] provide highly efficient detection of weak binders, often with excellent throughput and minimal experimental complexity. The added value of CIDNP-LLS, therefore does not lie in replacing established approaches, but in complementing them with a fundamentally different contrast mechanism. In addition, the use of competition-based assays, as demonstrated previously, can help mitigate the limitations in terms of chemical space inherent to CIDNP-LLS.

CIDNP-LLS may be particularly attractive for systems in which traditional contrast mechanisms become less discriminative, such as low-molecular-weight proteins, binding events that induce pronounced symmetry changes in the ligand, or targets with ill-defined binding pockets. In this context, the method may provide a useful tool for probing the drugability of IDPs, where global tumbling changes are minimal, but local or symmetry-related perturbations can be significant.

Materials and methods

Expression of His-AANAT

The plasmid encoding N-terminal His-tagged AANAT and kanamycin resistance was transformed into *E. coli* BL21(DE3) Star. For expression, two precultures (25 mL each) were grown overnight in LB medium at 37 °C. These were used to grow a ^{15}N labelled M9 minimal culture, which was incubated at 37 °C until reaching an optical density (OD_{600}) of 0.6. The temperature was reduced to 25 °C and expression was induced at OD_{600} = 0.75 by the addition of 1 mM IPTG, allowing growth to continue at 25 °C overnight. Cells were harvested by centrifugation, and the pellet was re-suspended in 20 mM Tris–HCl (pH 7.9), 500 mM NaCl, and 5 mM imidazole, 5 mM β-mercaptoethanol (BME). The suspension was filtered and lysed using a microfluidizer. Cellular debris were removed by centrifugation at 20 000 rpm for 30 min at 4 °C, followed by filtration of the supernatant. The lysate was applied to a Ni^{2+}-NTA affinity column equilibrated with the same buffer. The column was washed with lysis buffer to remove non-bound proteins. His-AANAT was eluted using lysis buffer containing 500 mM imidazole. The protein was concentrated to 500 μM and buffer-exchanged into NMR buffer (20 mM sodium phosphate, 100 mM NaCl, pH 7.0), flash frozen, and lyophilized for long-term storage. (Please note that the protein is not stable for more than 2 days in solution). All NMR experiments were performed in the NMR buffer containing 100% D_2O (pD = 7.0)

NMR experiments

All NMR experiments were carried out on a Bruker Avance III HD 600 MHz equipped with a Cryoprobe. All photo-CIDNP experiments were conducted using the commercial CRIO-X setup equipped with a 1.6 W laser at 520 nm.[26]

^{1}H-CIDNP and ^{1}H-CIDNP-PEARLScreen experiments were recorded with varying laser irradiation times and CPMG delays. Each spectrum was acquired with 16384 complex points in the direct dimension, corresponding to a total acquisition time of 0.85 s. The residual signal of water was suppressed using WATERGATE.[36] The intervals τ between the CPMG refocusing pulses were chosen to be 5 ms. Unless stated otherwise, 2 s of laser irradiation was applied before each scan.

SLIC-based experiments were acquired with delays $0.1 < \tau_{LLS} < 30$ s, 2 scans, and 16384 complex points in the direct dimension (acquisition time of 0.85 s). LLS for IPA was excited using a SLIC pulse length of 250 ms with an attenuation of 54.38 dB (*ca.* 29.6 Hz radio-frequency amplitude, near $2J^{\text{geminal}}$). In "on-the-fly" measurements, the duration of the second SLIC pulse was shortened by a factor N = 5 or 3, according to the number of LLS delays acquired, using 16 scans. For CIDNP-LLS experiments, a laser irradiation was applied for only 1 s before each scan to reduce bleaching effects, unless otherwise specified.

All photo-CIDNP measurements were performed in the presence of 5 mM glucose, 20 μM fluorescein, and 200 nM each of glucose oxidase and catalase, as previously reported.[37]

Peak picking and SNR determination for all experiments were performed using Mestrenova software (Mnova, Mestrelab Research). Data analysis was performed using Python.

[^{15}N, ^{1}H]-HSQC spectra of 120 μM AANAT were acquired with 200 × 2048 points (t_1^{max} = 41 ms, t_2^{max} = 0.121 s), and 44 scans per increment. The IPA concentrations were 0, 100, 250, 500, 1000, 2000, and 5000 μM. Peak picking was performed with CCPNMR 3.3.2.1,[38] and subsequent analysis was carried out in Python.

Chemical shift perturbations (CSPs) were calculated according to:[39]

$$\Delta\delta_{obs} = \sqrt{\frac{\left(\left(\delta_{obs,H} - \delta_{free,H}\right)^2 + \left(0.14\left(\delta_{obs,N} - \delta_{free,N}\right)\right)^2\right)}{2}} \quad (3)$$

where δ_{obs} and δ_{free} are the chemical shifts in the ^{1}H and ^{15}N dimensions of the [^{15}N, ^{1}H]-HSQC of the protein AANAT in the presence or absence of IPA. Dissociation constants were determined by fitting the observed CSPs to

$$\Delta\delta_{obs} = \Delta\delta_{max}\frac{K_D + L_{tot} + P_{tot} - \sqrt{\left(K_D + L_{tot} + P_{tot}\right)^2 - 4L_{tot}P_{tot}}}{2P_{tot}}, \quad (4)$$

where $\Delta\delta_{max}$ is the maximal chemical perturbation upon full

saturation of the protein, L_{tot} and P_{tot} are the total IPA and AANAT concentrations in the sample, and K_D is the dissociation constant of the complex of IPA and AANAT.

Conflicts of interest

The authors declare the following competing financial interests: co-authors M. B., F. T., and R. R. are co-founders of the company NexMR AG. None of the remaining authors declare any conflicts of interest.

Data availability

Other additional results are shown in the supplementary information (SI). Supplementary information: NMR data of Fig. 3 and 4 are available at Zenodo at https://doi.org/10.5281/zenodo.18743676. See DOI: https://doi.org/10.1039/D6CP00658B.

Acknowledgements

R.R. and M.B. acknowledge support from SNSF (200021L-232120). K.S. acknowledges support by l'Agence Nationale de la Recherche (ANR) on the project THROUGH-NMR (ANR-24-CE93-0011-01). GB acknowledges support by the European Research Council (ERC) for the Synergy grant "Highly Informative Drug Screening by Overcoming NMR Restrictions" (HISCORE, grant agreement number 951459).

References

1 J. H. Ardenkjaer-Larsen, B. Fridlund, A. Gram, G. Hansson, L. Hansson, M. H. Lerche, R. Servin, M. Thaning and K. Golman, Increase in signal-to-noise ratio of >10 000 times in liquid-state NMR, *Proc. Natl. Acad. Sci. U. S. A.*, 2003, **100**, 10158–10163.

2 C. R. Bowers and D. P. Weitekamp, Transformation of Symmetrization Order to Nuclear-Spin Magnetization by Chemical-Reaction and Nuclear-Magnetic-Resonance, *Phys. Rev. Lett.*, 1986, **57**, 2645–2648.

3 R. W. Adams, J. A. Aguilar, K. D. Atkinson, M. J. Cowley, P. I. Elliott, S. B. Duckett, G. G. Green, I. G. Khazal, J. Lopez-Serrano and D. C. Williamson, Reversible interactions with para-hydrogen enhance NMR sensitivity by polarization transfer, *Science*, 2009, **323**, 1708–1711.

4 J. Bargon and H. Fischer, Kernresonanz-Emissionslinien Wahrend Rascher Radikalreaktionen. 2. Chemisch Induzierte Dynamische Kernpolarisation, *Z. Naturforsch., Astrophys. Phys. Phys. Chem.*, 1967, **A22**, 1556.

5 H. R. Ward and R. G. Lawler, Nuclear Magnetic Resonance Emission and Enhanced Absorption in Rapid Organometallic Reactions, *J. Am. Chem. Soc.*, 1967, **89**, 5518.

6 J. Eills, D. Budker, S. Cavagnero, E. Y. Chekmenev, S. J. Elliott, S. Jannin, A. Lesage, J. Matysik, T. Meersmann, T. Prisner, J. A. Reimer, H. Yang and I. V. Koptyug, Spin Hyperpolarization in Modern Magnetic Resonance, *Chem. Rev.*, 2023, **123**, 1417–1551.

7 M. H. Levitt, Long live the singlet state!, *J. Magn. Reson.*, 2019, **306**, 69–74.

8 M. Carravetta, O. G. Johannessen and M. H. Levitt, Beyond the ${T}_{1}$ Limit: Singlet Nuclear Spin States in Low Magnetic Fields, *Phys. Rev. Lett.*, 2004, **92**, 153003.

9 N. Salvi, R. Buratto, A. Bornet, S. Ulzega, I. Rentero Rebollo, A. Angelini, C. Heinis and G. Bodenhausen, Boosting the Sensitivity of Ligand–Protein Screening by NMR of Long-Lived States, *J. Am. Chem. Soc.*, 2012, **134**, 11076–11079.

10 R. Buratto, D. Mammoli, E. Chiarparin, G. Williams and G. Bodenhausen, Exploring Weak Ligand–Protein Interactions by Long-Lived NMR States: Improved Contrast in Fragment-Based Drug Screening, *Angew. Chem., Int. Ed.*, 2014, **53**, 11376–11380.

11 R. Buratto, D. Mammoli, E. Canet and G. Bodenhausen, Ligand–Protein Affinity Studies Using Long-Lived States of Fluorine-19 Nuclei, *J. Med. Chem.*, 2016, **59**, 1960–1966.

12 A. K. Grant and E. Vinogradov, Long-lived states in solution NMR: Theoretical examples in three- and four-spin systems, *J. Magn. Reson.*, 2008, **193**, 177–190.

13 P. Ahuja, R. Sarkar, P. R. Vasos and G. Bodenhausen, Long-lived States in Multiple-Spin Systems, *Chem. Phys. Chem.*, 2009, **10**, 2217–2220.

14 G. Stevanato, S. S. Roy, J. Hill-Cousins, I. Kuprov, L. J. Brown, R. C. D. Brown, G. Pileio and M. H. Levitt, Long-lived nuclear spin states far from magnetic equivalence, *Phys. Chem. Chem. Phys.*, 2015, **17**, 5913–5922.

15 A. Sonnefeld, G. Bodenhausen and K. Sheberstov, Polychromatic Excitation of Delocalized Long-Lived Proton Spin States in Aliphatic Chains, *Phys. Rev. Lett.*, 2022, **129**, 183203.

16 S. J. DeVience, R. L. Walsworth and M. S. Rosen, Preparation of Nuclear Spin Singlet States Using Spin-Lock Induced Crossing, *Phys. Rev. Lett.*, 2013, **111**, 173002.

17 A. Sonnefeld, A. Razanahoera, P. Pelupessy, G. Bodenhausen and K. Sheberstov, Long-lived states of methylene protons in achiral molecules, *Sci. Adv.*, 2022, **8**, eade2113.

18 A. Bornet, S. Jannin and G. Bodenhausen, Three-field NMR to preserve hyperpolarized proton magnetization as long-lived states in moderate magnetic fields, *Chem. Phys. Lett.*, 2011, **512**, 151–154.

19 M. C. D. Tayler, I. Marco-Rius, M. I. Kettunen, K. M. Brindle, M. H. Levitt and G. Pileio, Direct Enhancement of Nuclear Singlet Order by Dynamic Nuclear Polarization, *J. Am. Chem. Soc.*, 2012, **134**, 7668–7671.

20 A. Razanahoera, A. Sonnefeld, K. Sheberstov, P. Narwal, M. Minaei, K. Kouřil, G. Bodenhausen and B. Meier, Hyperpolarization of Long-Lived States of Protons in Aliphatic Chains by Bullet Dynamic Nuclear Polarization, Revealed on the Fly by Spin-Lock-Induced Crossing, *J. Phys. Chem. Lett.*, 2024, **15**, 9024–9029.

21 R. Kaptein and L. J. Oosterhoff, Chemically induced dynamic nuclear polarization III (anomalous multiplets of radical coupling and disproportionation products), *Chem. Phys. Lett.*, 1969, **4**, 214–216.

22 F. R. Torres, Exploration of the close chemical space of tryptophan and tyrosine reveals importance of hydrophobicity in CW-photo-CIDNP performances, *Magn. Reson.*, 2021, **2**, 321–329.
23 F. Torres, M. Butikofer, G. R. Stadler, A. Renn, H. Kadavath, R. Bobrovs, K. Jaudzems and R. Riek, Ultrafast Fragment Screening Using Photo-Hyperpolarized (CIDNP) NMR, *J. Am. Chem. Soc.*, 2023, **145**(22), 12066–12080.
24 G. R. Stadler, T. F. Segawa, M. Bütikofer, V. Decker, S. Loss, B. Czarniecki, F. Torres and R. Riek, Fragment Screening and Fast Micromolar Detection on a Benchtop NMR Spectrometer Boosted by Photoinduced Hyperpolarization, *Angew. Chem., Int. Ed.*, 2023, **62**(40), e202308692.
25 M. Bütikofer, G. R. Stadler, H. Kadavath, R. Cadalbert, F. Torres and R. Riek, Rapid Protein–Ligand Affinity Determination by Photoinduced Hyperpolarized NMR, *J. Am. Chem. Soc.*, 2024, **146**, 17974–17985.
26 W. Wüster, P. Gebbers, A. Renn, M. Bütikofer, R. Riek and F. Torres, An automated NMR platform with light-coupled cryogenic probes to detect low micromolar samples, *Magn. Reson. Discuss.*, 2024, 1–10.
27 K. F. Sheberstov, L. Chuchkova, Y. Hu, I. V. Zhukov, A. S. Kiryutin, A. V. Eshtukov, D. A. Cheshkov, D. A. Barskiy, J. W. Blanchard, D. Budker, K. L. Ivanov and A. V. Yurkovskaya, Photochemically Induced Dynamic Nuclear Polarization of Heteronuclear Singlet Order, *J. Phys. Chem. Lett.*, 2021, **12**, 4686–4691.
28 D. R. Dempsey, K. A. Jeffries, J. D. Bond, A.-M. Carpenter, S. Rodriguez-Ospina, L. Breydo, K. K. Caswell and D. J. Merkler, Mechanistic and Structural Analysis of Drosophila melanogaster Arylalkylamine N-Acetyltransferases, *Biochemistry*, 2014, **53**, 7777–7793.
29 N. Lorz, B. Czarniecki, S. Loss, B. Meier and A. D. Gossert, Higher Contrast in 1H-Observed NMR Ligand Screening with the PEARLScreen Experiment, *Angew. Chem., Int. Ed.*, 2025, **64**, e202423879.
30 S. Stob and R. Kaptein, Photo-Cidnp of the Amino Acids, *Photochem. Photobiol.*, 1989, **49**, 565–577.
31 F. Torres, A. Sobol, J. Greenwald, A. Renn, O. Morozova, A. Yurkovskaya and R. Riek, Molecular features toward high photo-CIDNP hyperpolariztion explored through the oxidocyclization of tryptophan, *Phys. Chem. Chem. Phys.*, 2021, **23**, 6641–6650.
32 H. Yang, M. F. Mecha, C. P. Goebel and S. Cavagnero, Enhanced nuclear-spin hyperpolarization of amino acids and proteins *via* reductive radical quenchers, *J. Magn. Reson.*, 2021, **324**, 106912.
33 C. Bengs, L. Dagys, G. A. I. Moustafa, J. W. Whipham, M. Sabba, A. S. Kiryutin, K. L. Ivanov and M. H. Levitt, Nuclear singlet relaxation by chemical exchange, *J. Chem. Phys.*, 2021, **155**, 124311.
34 M. Mayer and B. Meyer, Characterization of Ligand Binding by Saturation Transfer Difference NMR Spectroscopy, *Angew. Chem., Int. Ed.*, 1999, **38**, 1784–1788.
35 C. Dalvit, G. Fogliatto, A. Stewart, M. Veronesi and B. Stockman, WaterLOGSY as a method for primary NMR screening: Practical aspects and range of applicability, *J. Biomol. NMR*, 2001, **21**, 349–359.
36 M. Liu, X. Mao, C. Ye, H. Huang, J. K. Nicholson and J. C. Lindon, Improved WATERGATE Pulse Sequences for Solvent Suppression in NMR Spectroscopy, *J. Magn. Reson.*, 1998, **132**, 125–129.
37 Y. Okuno and S. Cavagnero, Fluorescein: A Photo-CIDNP Sensitizer Enabling Hypersensitive NMR Data Collection in Liquids at Low Micromolar Concentration, *J. Phys. Chem. B*, 2016, **120**, 715.
38 S. P. Skinner, R. H. Fogh, W. Boucher, T. J. Ragan, L. G. Mureddu and G. W. Vuister, CcpNmr AnalysisAssign: a flexible platform for integrated NMR analysis, *J. Biomol. NMR*, 2016, **66**, 111–124.
39 M. P. Williamson, Using chemical shift perturbation to characterise ligand binding, *Prog. Nucl. Magn. Reson. Spectrosc.*, 2013, **73**, 1–16.